Ceramic monolith- and foam-structured catalysts via in-situ combustion deposition for energetic applications

Cristina Italiano*, Lidia Pino, Massimo Laganà, Antonio Vita

CNR-ITAE "Nicola Giordano", Salita S. Lucia sopra Contesse 5, 98126, Messina, Italy

cristina.italiano@itae.cnr.it

ABSTRACT. *In this work, the Me/CeO_2 (Me = Rh, Ni) catalytic phase was in-situ deposited by the Solution Combustion Synthesis (SCS) on commercial cordierite monolith (500 cpsi) and alumina open-cell foams (20,30,40 ppi). All the coated structures were characterized by SEM/EDX to analyze the morphological characteristics of the coated films; the mechanical stability was analyzed by ultrasound tests; pressure drops at different superficial velocities were derived. The catalytic activity and stability were investigated towards Steam Reforming (SR) and Oxy-Steam Reforming (OSR) of different fuels (CH_4, biogas, n-dodecane) and CO_2 methanation reaction. High catalytic activity was observed for both reforming and methanation processes, following the order 500 cpsi-monolith < 20 ppi-foam < 30 ppi-foam ≈ 40 ppi-foam. Excellent long-term stability was observed over 200 h of time-on-stream (TOS).*

RÉSUMÉ. *Dans cet article, la phase catalytique Me/CeO_2 (Me = Rh, Ni) a été déposée in situ par la synthèse de combustion en solution (SCS, le sigle de « Solution Combustion Synthesis » en anglais) sur des monolithes de cordiérite (500 cpsi) et des mousses à cellules ouvertes d'alumine (20,30,40 ppi). Toutes les structures revêtues ont été caractérisées par SEM / EDX pour analyser les caractéristiques morphologiques des films revêtus; la stabilité mécanique a été analysée par ultrasons; la perméabilité et le coefficient de forme ont été dérivés des données de chute de pression. L'activité et la stabilité catalytique ont été étudiées pour les réactions de reformage à la vapeur (SR, le sigle de « Steam Reforming » en anglais) et à l'oxy-vapeur (OSR, le sigle de « Oxy-Steam Reforming » en anglais) de différents combustibles (CH_4, biogaz, n-dodécane) et la réaction de méthanisation au CO_2. Une activité catalytique élevée a été observée à la fois pour les procédés de reformage et de méthanation, suivant l'ordre de 500 cpsi-monolithe <20 ppi-mousse <30 ppi-mousse ≈ 40 ppi-mousse. Une excellente stabilité à long terme a été observée sur une période de 200 heures d'utilisation (TOS, le sigle de « time-on-stream » en anglais).*

KEYWORDS: *monolith, open-cell foam, methanation, reforming, structured catalysts.*

MOTS-CLÉS: *monolithe, mousse à cellules ouvertes, méthanisation, reformage, catalyseurs structurés.*

DOI:10.3166/ACSM.42.405-418

1. Introduction

Process intensification (PI) is a promising strategy to develop more competitive and sustainable processes in a transition towards a bio-based economy (Curcio, 2013). The most interesting technological approach in heterogeneous catalysis is the application of structured catalysts (e.g. monoliths and foams) which are characterized by large surface-to-volume ratio, good heat and mass transfer properties, allowing the use of small and compact reactors, interesting for small-scale applications (Williams, 2001; Borreani *et al.*, 2017). Indeed, monolith- and foam-structured catalysts are widely used in environmental applications for both automotive and stationary emission control (Ercolino *et al.*, 2017). Moreover, they are increasingly under development for many reaction applications, such as highly endothermic and exothermic reactions (hydrogenation, combustion or reforming processes) (Groppi *et al*., 2005).

In this paper, we investigated the catalytic activity of structured catalysts towards several applications, i.e. Steam Reforming (SR) and Oxy-Steam Reforming (OSR) of different fuels (CH_4, biogas, n-dodecane) and CO_2 methanation reaction. The catalytic phase was in-situ deposited by the Solution Combustion synthesis (SCS) on commercial cordierite monoliths (500 cpsi) and alumina open-cell foams (20,30,40 ppi). The catalytic performances were investigated at atmospheric pressure varying temperature and space velocity. Stability tests over 200 h of time-on-stream were also performed.

2. Experimental

2.1. Catalysts preparation and characterization

Me/CeO_2 catalyst (Me = Rh, Ni) were *in-situ* deposited on ceramic monolith (MO) and open-cell foam (OCF), according to the procedure elsewhere described (Specchia *et al.*, 2017; Vita *et al.*, 2015; Vita *et al.*, 2018). The main geometrical characteristics of bare supports are listed in Table 1. The characteristic sizes (d_p) are the channel inner size (monolith) and the pore diameter (foam). Monolith channel inner size (d_p) and wall thickness (t) were microscopically determined by using 30 different supports. Foam pore diameter (d_p) and strut thickness (t) were microscopically determined by using ca. 500 features of 30 different supports. Bed porosity (V_p) was determined by helium pycnometry. The open frontal area (ε) of monolithic support was calculated from channel inner size (d_p) and wall thickness (t) by equation $\varepsilon = d_p^2/(d_p + t)^2$. Foam open frontal area was calculated from the relative density (ρ_A/ρ_B) by the equation

$$\varepsilon = 1 - \rho_A/\rho_B = 1 - 2.59\left[t/(t + d_p)^2\right].$$

Monolith geometric surface area (GSA) was calculated according to Cybulski and Moulijn (Cybulsk & Moulijn, 1994), while the tetrakaidecahedron model of

Buciuman and Kraushaar-Czarnetzki (Buciuman & Kraushaar-Czarnetzki, 2003) was used for the foam.

Table 1. Geometric properties of bare supports

	d_p (mm)	t (mm)	V_p *(%)*	ε(-)	GSA (m^{-1})
500 cpsi - MO	0.83	0.32	72.5	0.52	2529
20 ppi - OCF	1.92	0.51	85.1	0.89	669
30 ppi - OCF	1.40	0.41	83.6	0.87	967
40 ppi - OCF	1.07	0.33	82.5	0.86	1292

Commercial cordierite monoliths and alumina foams were washed in water/acetone (50/50 Vol.%) ultrasonic bath for 30 min and dried at 120°C for 2 h. The catalytic layers were in situ deposited by SCS dipping each structure in an aqueous solution containing metal precursors and urea (as fuel). The wet supports were introduced into a furnace preheated at 600°C for ca. 10 min, where the combustion reaction occurred, and rapidly cooled down to room temperature in few min. The deposition steps were repeated several times to reach the total loading of ca. 0.2 g/cm^3.

A U-tube manometer connected to the reactor containing the OCFs was used measure the pressure drop at different superficial velocities. N_2 flow was supplied at ambient temperature by a mass flow-meter (*Brooks Instrument*) and measured by a digital flow-meter (*Agilent ADM 2000*).

The coating procedure was evaluated in terms of homogeneity of the coating and adhesion force. Scanning electron microscopy (SEM) images were obtained using a *FEI XL 30* equipped with field emission gun. The structured samples were cut longitudinally to evaluate the thickness of the catalytic layer. The adherence of the coating was evaluated in terms of weight loss after two ultrasonic treatment in 50 Vol.% isopropyl alcohol solution. The coated structures were treated for 30 min at 45 kHz and 130W using the USC 900D ultrasonic bath.

Transmission electron microscopy (TEM) micrographs were obtained using a *Philips CM12 instrument*. The reduced coating layer was scraped from the structures walls, dispersed in isopropyl alcohol by ultrasonic treatment, and placed on holey copper grids.

2.2. Catalytic tests

Catalytic tests were carried out in a quartz fixed-bed reactor (i.d. = 1 cm) inserted into a furnace equipped with a PID temperature controller. High purity gases (99.999%, from Rivoira) were used in the experiments, keeping constant the flow rates by mass flow-controllers (Brooks Instrument Smart Mass Flow). Steam was fed using an isocratic pump (Agilent 1100 Series) and a specially designed

evaporator. The reaction temperature was measured at the centre of the catalyst bed using a chromel/alumel thermocouple. Moreover, two thermocouples were positioned at the inlet and at the outlet of the catalytic bed respectively to measure the gradient temperature generated by reactions. SR and OSR experiments were carried out varying temperature, space velocity, S/C and O/C molar ratios, as reported in Table 2. Methanation experiments were carried out at fixed H_2/CO_2 ratio of 4, varying temperature (T = 300-600°C) and space velocity (10,000-50,000 h^{-1}).

The duration of each test was set to 6 h (activity test) and 200 h (stability test). Before the catalytic test, the catalysts were reduced in a flow of 50% H_2 in N_2 (30 Nml/min) at 200°C (noble metals-based catalyst) and 600°C (Ni-based catalyst) for 1 h. The composition of reagents and products was determined using an on-line gas chromatograph (*Agilent 5975C series 4C/MSD*) equipped with TCD and FID detectors and mass spectrometer. CH_4, revealed in both detectors, was used as reference compound, while N_2 was used as internal standard for mass balance calibration.

Chemical composition in thermochemical equilibrium was obtained by the HSC Chemistry 7.1® calculation software, using the Gibbs free-energy minimization method.

Table 2. Experimental conditions for SR and OSR tests

Fuel	Steam Reforming (SR)			
	T (°C)	S/C	O/C	GHSV (h^{-1})
CH_4	700-900	1-5	-	5,000-60,000
Biogas	700-900	1-5	-	5,000-60,000
Diesel	700-800	1-2.5	-	16,000-40,000
	Oxy-Steam Reforming (OSR)			
	T (°C)	S/C	O/C	GHSV (h^{-1})
CH_4	600-900	0.3-2.5	0.45-0.75	5,000-60,000
Biogas	600-900	0.3-2.5	0.1-0.2	5,000-60,000
Diesel	700-800	1-2.5	0.2-0.6	16,000-40,000

Notes: Simulated biogas (CH_4/CO_2 = 0.6666) and diesel (n-$C_{12}H_{26}$) were used for the catalytic tests.

3. Results and discussion

3.1. Catalysts characterization

Pressure drop of the studied structures was measured at different superficial velocities and the results are presented in Figure 1. The experimental results well fitted the Hagen-Poiseuille and Lacroix theoretical calculations for MO and OCFs,

respectively. Moreover, the measured pressure drop followed the order 500cpsi-MO < 20ppi-OCF < 30ppi-OCF < 40ppi-OCF structures. However, pressure drop lower than packed-bed systems allowed for higher catalyst utilization and improved catalytic activity (Arunachalam & Edwin, 2017).

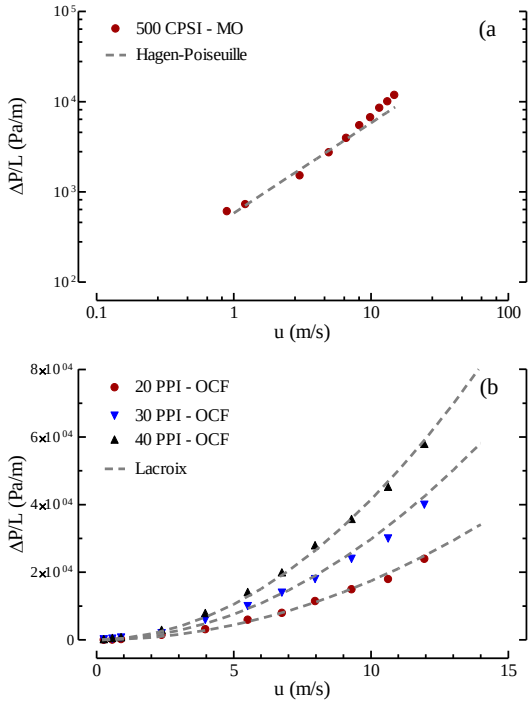

Figure 1. Pressure drop measurements for monolith (a) and foams (b) compared to Hagen-Poiseuille and Lacroix theoretical calculations

Figures 2 and 3 show SEM images of bare and coated monoliths and foams. A reduction of the macro-porosity of cordierite (Fig. 2a) and alumina (Fig. 3a) was revealed after the in-situ deposition of the catalytic layer (Figs. 2b and 3b). Well uniform coating layers were found, as evidenced by the EDX mapping of the coated monolith (Figs. 2c,d) and foam (Figs. 3c,d). Moreover, the magnification of the coated layer (Figs. 2e and 3e) confirmed the presence of a significant residual porosity due to the escaped gas during the SCS step. Average thickness of ca. 10-40 μm (Figs. 2f and 3f) were determined.

The mechanical resistance of the coated layers, evaluated by ultrasonic treatment in isopropyl alcohol solution, evidenced good adherence of the catalytic layer to the cordierite support. Negligible weight loss of ca. 0.3-0.5% after the second adhesion test (calculated on the total weight of the monolith) were found. The good resistance

to mechanical stress of the coated layer could be ascribed to cordierite and alumina macropores in which catalyst particles penetrated, ensuring good adhesion of the catalytic layer.

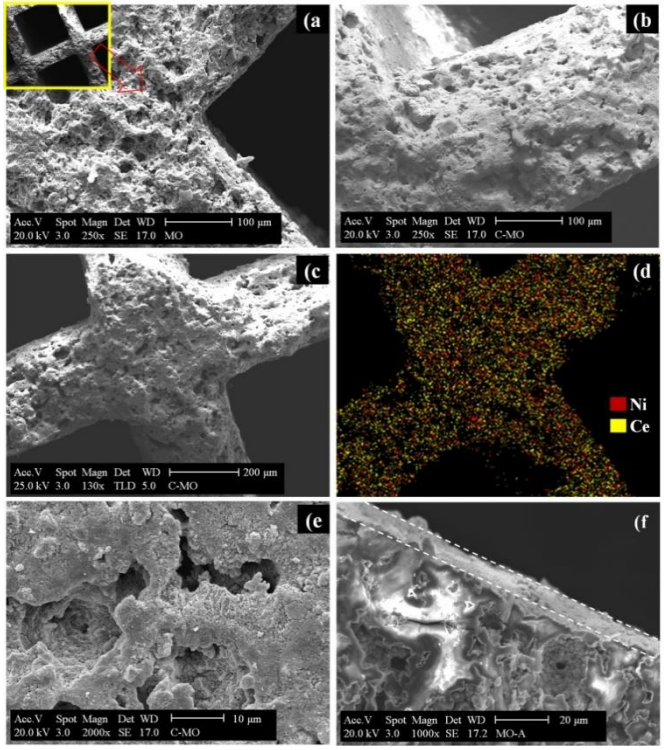

Figure 2. SEM micrographs of bare (a) and Ni/CeO_2-coated (b-f) MO. SEM micrographs at different magnification (c,e) and corresponding EDX mapping (d). Cross section for catalytic layer view (f)

The morphology of catalyst was checked by TEM analysis. TEM images in Figure 4 showed 30-50 nm CeO_2 particles in agglomerate form. Finely dispersed and well distributed Me (Me = Ni, Rh) particles were revealed.

3.2. SR and OSR activity

The two primary catalytic processes for converting hydrocarbons into carbon monoxide and hydrogen are steam reforming (SR) and partial oxidation (POX). Oxy-Steam reforming (OSR) is a hybrid process that combines the exothermic POX and the endothermic SR. In reality, OSR produces both CO and CO_2, due to the presence of excess water providing a pathway for the water gas shift (WGS) reaction (Bereketidou & Goula, 2012; Song & Pan, 2004).

POX: $C_nH_m + 1/2nO_2 \rightarrow nCO + 1/2mH_2$

SR: $C_nH_m + nH_2O \rightarrow nCO + (2+1/2m)\ H_2$

OSR: $C_nH_m + xO_2 + (n-2x)\ H_2O \rightarrow nCO + (n-2x+1/2m)\ H_2$

WGS: $CO + H_2O \leftrightarrow CO_2 + H_2$

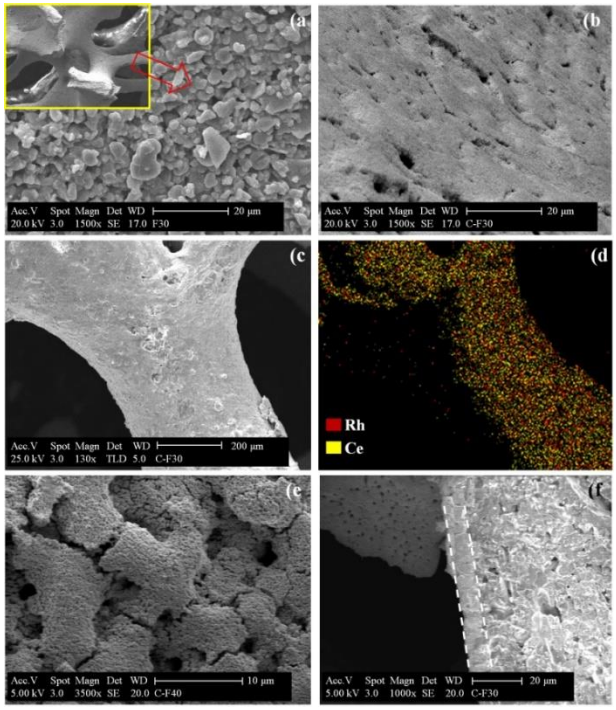

Figure 3. SEM micrographs of bare (a) and Rh/CeO_2-coated (b-f) OCF. SEM micrographs at different magnification (c,e) and corresponding EDX mapping (d). Cross section for catalytic layer view (f)

Carbon and coke deposition are major problems in reforming processes (Parmar, 2009). Coke is produced by thermal cracking of high molecular weight hydrocarbons (i.e. n-$C_{12}H_{26}$) through the following sequence. Depending on the condition amorphous (filamentous) carbon (T<600°C) or graphitic (whisker) carbon (T>600°C) are formed.

$C_{12}H_{26}$ → Olefins → Polymers → Coke → Amorphous carbon → Graphitic carbon

Moreover, carbon is also produced by Boudouard reaction, reverse gasification and methane decomposition:

$2CO \rightarrow C + CO_2$

$CO + H_2 \rightarrow C + H_2O$

$CH_4 \leftrightarrow C + 2H_2$

Carbon and coke formation could cause degradation of the reformer performance and reduce its lifetime significantly (Achouri *et al*., 2013). However, the presence of steam and/or oxygen can dramatically reduce or eliminate carbon formation by coke reforming and coke oxidation reactions:

$C + H_2O \rightarrow CO + H_2$

$C + O_2 \rightarrow CO_2$

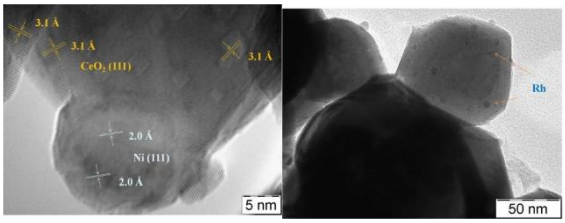

Figure 4. TEM images of Me/CeO_2 catalytic layers scraped from different internal walls of monoliths and foams

Figure 5 shows the influence of space velocity on the activity of Rh- and Ni-based structured catalysts towards CH_4 OSR reaction. High activity was observed for the Rh-based catalyst, showing high CH_4 conversion (98.3%) and H_2 concentration (67.9%) at 400,000 Nml·g-1·h−1. Contrarily, Ni-based monolith showed a noticeable performance decay. Indeed, CH_4 conversion decreased from ca. 99% to 62% by increasing the space velocity from ca. 40,000 to 400,000 Nml·g-1·h−1. As previously reported, this was due to Ni sintering and mainly carbon deposition phenomena, as evidenced in Figure 6, where encapsulated Ni particles and filamentous whiskers were evidenced (Kim *et al.*, 2000).

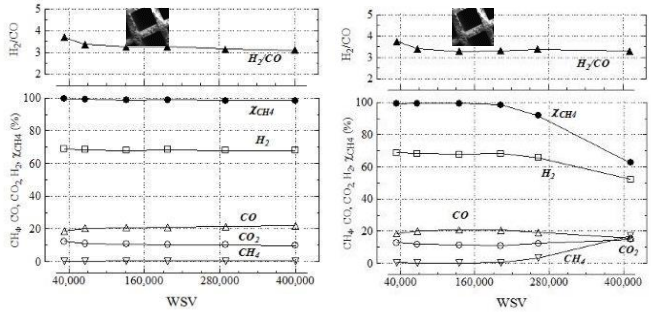

Figure 5. Influence of space velocity on CH_4 OSR activity of (a) Rh/CeO_2 and (b) Ni/CeO_2 supported on monolith (Reaction conditions: T= 800°C, O/C = 0.55, S/C = 1.2)

Figure 7 shows the influence of space velocity on the biogas OSR activity over Rh/CeO_2 catalyst supported on OCFs with different pore density (20-40 ppi). The decrease in catalytic activity by increasing the space velocity was less pronounced as the pore density increased to 30 ppi (Figure 7b) and 40 ppi (Figure 7c). Indeed, F30 and F40 catalysts showed almost total (<99%) and stable CH_4 conversion at all the investigated conditions. This evidence could be attributed to the increase in exposed surface area by increasing the pore density (Table 1). Thus, the following activity order was derived towards the biogas SR reaction: F20 < F30 ≈ F40 (Zeppieri *et al.*, 2010).

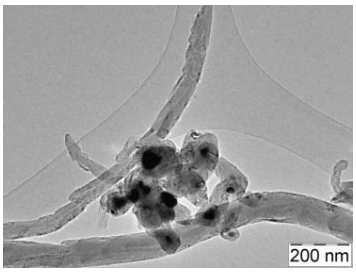

Figure 6. TEM images of used Ni/CeO_2 catalyst scraped from internal wall of monolith

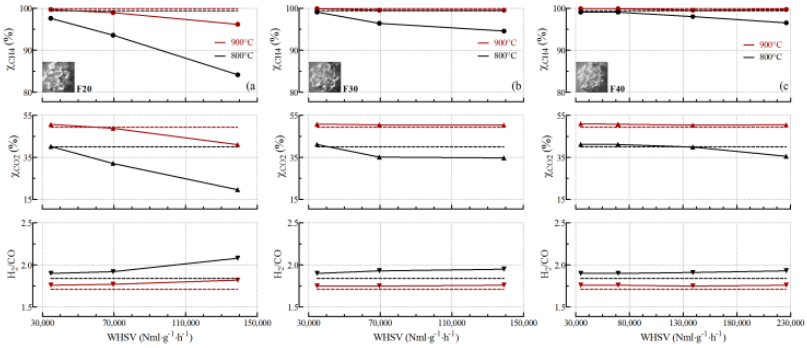

Figure 7. Influence of space velocity on biogas OSR activity of Rh/CeO_2 supported on 20 (a), 30 (b) and 40 ppi (c) OCFs (Reaction conditions: T= 800-900°C, O/C = 0.2, S/C = 1)

A special bed configuration with an optimized temperature-control was adopted for n-dodecane SR experiments in order to avoid/minimize carbon formation due to cracking phenomena, especially at the inlet of the catalytic bed. The temperature gradient (ca. 500–800 ◦C) along the catalytic bed played a key role in determining final products concentration. Table 3 summarizes the activity results obtained with

Rh/CeO_2 catalyst supported on monolith. Total n-dodecane conversion was observed at all the investigated S/C ratios, while H_2/CO ratio increased from ca. 3 to 5, while remaining higher than equilibrium prediction (2.6-4.2) due to the contribute of WGS and methanation ($CO_2 + 4H_2 \leftrightarrow CH_4 + 2H_2O$) reactions (Vita *et al*., 2016; Dagle *et al.*, 2011).

Table 3. Influence of S/C on n-dodecane SR activity of Rh/CeO_2 supported on monolith (Reaction conditions: T= 500-800°C, GHSV=33,000 h^{-1})

S/C	Products composition (%)					H_2/CO
	CO_2	H_2O	H_2	CO	CH_4	
1.5	6.3	15.9	58.4	18.9	0.5	3.1
2.5	7.8	31.4	49.3	11.5	0.0	4.3
3.0	8.9	35.2	46.7	9.2	0.0	5.1

Characterization data and reforming results of the Rh-based catalyst supported on monolith and foam structures made it a promising active-stable catalyst for reforming processes.

3.3. Methanation activity

The production of Substitute Natural Gas (SNG) by CO_2 methanation, also called Sabatier reaction, proceeds according to (Li *et al*., 2015):

$CO_2+4H_2 \leftrightarrow CH_4+2H_2O$

It is a reaction of great technological and environmental potential, leading to (i) storage of excess H_2 generated from renewable energy, (ii) reduction of CO_2 emissions (greenhouse gas) from the atmosphere and (iii) production of SNG whose distribution infrastructures are readily available (Duyar *et al.*, 2015). CO_2 methanation is a strongly exothermic reaction that results in large potential temperature increases and hot spot formation, lowering the yield and leading to catalyst deactivation by sintering and carbon deposition (Rostrup-Nielsen *et al*., 2007).

Figure 8 shows the CH_4 productivity (hourly methane produced per unit weight of catalyst) obtained with structured catalyst as a function of reaction temperature and space velocity. The activity of the studied system increased by increasing the temperature, reaching the maximum at ca. 450–500°C and decreasing afterward (Figure 8a). Indeed, low temperatures were thermodynamically beneficial to the reaction but kinetically disadvantage due to the great kinetic barrier for the full reduction of CO_2 (+4) to CH_4 (-4), an eight-electron process which required high activation energy (Xu *et al*., 2017). Further increase in the reaction temperature led to a slight decrease in the CH_4 productivity due to thermodynamic limit of methanation reaction and to the occurrence of reverse WGS reaction (Fukuhara *et*

al., 2017). Moreover, the CH_4 productivity increased by increasing the space velocity, reaching the highest value (10.7 $L_{CH4}\cdot g^{-1}\cdot h^{-1}$) at 400°C and 50,000 h^{-1}.

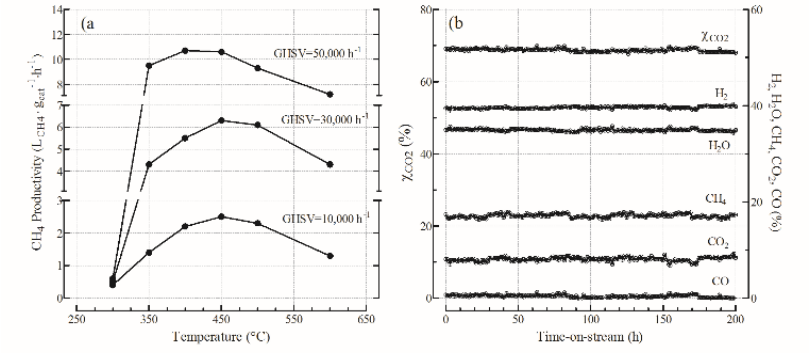

Figure 8. Influence of space velocity on methanation activity of Ni/Gd_2O_3-CeO_2 supported on monolith (a); Stability results over 200 h of TOS (b)

A long-term test was carried out at T=400°C and GHSV=30,000 h^{-1}, and the results are shown in Figure 8b. Stable performance, both in term of CO_2 conversion (68–69%) and effluent composition over 200 h of time-on stream, were obtained, confirming the high stability of the studied system.

Finally, higher activity was observed over OCFs structures, mainly due to the tortuous structure of the systems, which provide faster radial heat and mass transport with higher contacting efficiency than monolithic catalyst (Sadykov *et al*., 2015).

3.4. Evaluation of mass transfer limitations

The catalytic reaction between reactant molecules and active sites, generally located inside the catalyst pores, takes place after the reactant molecules diffuse from gas phase to the catalyst surface (external diffusion) and through the pores of the coated layer (internal diffusion). Thus, three operating regimes, namely kinetic, external mass transfer, and internal diffusion, can control the catalytic processes (Wijaya *et al*., 2012).

To estimate the influence of external and internal mass transfer limitation, the Carberry (Ca) and Weisz-Prater (WP) numbers were calculated according to the following equations (Ercolino *et al*., 2017; Dekker *et al*., 1995):

$$Ca = \frac{R_{obs}}{k_G \cdot GSA \cdot C_s} < \frac{0.05}{n}$$

$$WP = \frac{r_{obs} \cdot \rho_c \cdot \delta_c^2}{D_{s,e} \cdot C_s} < \frac{n+1}{2}$$

where R_{obs} (kmol·m^{-3}·s^{-1}) is the observed volumetric reaction rate for CH_4 (reforming processes) or CO_2 (methanation reaction); k_G (m·s^{-1}) is the mass transfer coefficient calculated from Sherwood (Sh), Reynold (Re) and Schmidt (Sc) dimensionless numbers; C_s (kmol·m^{-3}) is the concentration of CH_4 (reforming processes) or CO_2 (methanation reaction) in the feed mixture; r_{obs} (kmol·kg^{-1}·s^{-1}) is the observed reaction rate per unit weight of catalytic phase; ρ_c (kg·m^{-3}) is the density of the catalytic layer; δ_c (m) is the coated layer thickness; $D_{s,e}$ (m^2·s^{-1}) is the effective diffusivity of CH_4 or CO_2 in the coated layer.

Under the selected reaction conditions, the calculated Ca and WP numbers for a first-order reaction rate (n=1) were much lower than 0.05 and 1, respectively, confirming the absence of both external and internal mass transfer limitations.

4. Conclusions

Ceramic monolith (MO) and open-cell foam (OCF) as structured catalyst supports are increasingly under development for many reaction applications, due to i) high surface-to-volume ratio, ii) lower pressure drop, iii) faster mass/heat transfer and iv) higher contacting efficiency than packed bed reactors. In this paper, a brief outlook on structured catalyst employment for energetic applications (reforming and methanation reactions) was provided.

Structured catalysts were synthesized by the solution combustion synthesis (SCS), providing very uniform, thin and reproducible catalytic layers. The ultrasound adherence tests confirmed the excellent resistance of the coated layers to the mechanical stress, with weight loss always lower than 0.5%. High activity and excellent stability were observed. The tortuous structure of ceramic open-cell foam (OCF) provided a fast radial heat and mass transport with higher contacting efficiency, positively affecting the catalytic performances towards reforming processes and methanation reaction.

In this direction, it was demonstrated that structured catalysts emerge as a viable solution in the process intensification aimed at transforming conventional chemical processes into more economical, productive and green processes.

References

Achouri E., Abatzoglou N., Fauteux-Lefebvre C., Braidy N. (2013). Diesel steam reforming: Comparison of two nickel aluminate catalysts prepared by wet-impregnation and co-precipitation. *Catal. Today*, Vol. 207, pp. 13-20. https://doi.org/10.1016/j.cattod.2012.09.017

Arunachalam U. P., Edwin M. (2017). Theoretical investigation of a ceramic monolith heat exchanger using silicon carbide and aluminium nitride as heat exchanger material. *IJHT*, Vol. 35, pp. 645-650. https://doi.org/10.18280/ijht.350323

Bereketidou O. A., Goula M. A. (2012). Biogas reforming of syngas production over nickel supported on ceria-alumina catalysts. *Catal. Today*, Vol. 195, No. 1, pp. 93-100. https://doi.org/10.1016/j.cattod.2012.07.006

Borreani W., Bruzzone M., Chersola D., Firpo G., Lomonaco G., Palmero M., Panza F., Ripani M., Saracco P, Viberti C. M. (2017). Preliminary thermal-fluid-dynamic assessment of an ADS irradiation facility for fast and slow neutrons. *IJHT*, Vol. 35, pp. S186-S190. https://doi.org/10.18280/ijht.35Sp0126

Buciuman F., Kraushaar-Czarnetzki B. (2003). Ceramic foam monoliths as catalyst carriers. 1. Adjustment and description of the morphology. *Ind. Eng. Chem. Res.*, Vol. 42, No. 9, pp. 1863-1869. https://doi.org/10.1021/ie0204134

Curcio S. (2013). Process intensification in the chemical industry: A review. in *Sustainable development in chemical engineering: Innovative technologies*, 1st ed., V. Piemonte, M. De Falco and A. Basile. *John Wiley & Sons*, pp. 95-118. http://dx.doi.org/10.1002/9781118629703.ch5

Cybulski A., Moulijn J. A. (1994). Modelling of heat transfer in metallic monoliths consisting of sinusoidal cells. *Chem. Eng. J.*, Vol. 49, No. 1, pp. 19-27. https://doi.org/10.1016/0009-2509(94)85030-5

Dagle R. A., Karim A., Li G., Su Y., King D. L. (2011). Syngas conditioning. in *Fuel cells: Technologies for fuel processing*, D. Shekhawat, J.J. Spivey, D.A. Berry, *Elsevier*, pp. 361-408. http://dx.doi.org/10.1016/B978-0-444-53563-4.10012-4

Dekker F. H., Bliek A., Kapteijn F., Moulijn J. A. (1995). Analysis of mass and heat transfer in transient experiments over heterogeneous catalysts. *Chem. Eng. Sci.*, Vol. 50, pp. 3573-3580. https://doi.org/10.1016/0009-2509(95)00210-V

Duyar M. S., Ramachandran A., Wang C., Farrauto R. J. (2015). Kinetics of CO_2 methanation over Ru/γ-Al_2O_3 and implications for renewable energy storage applications. *J. CO_2 Util.*, Vol. 12, pp. 27-33. https://doi.org/10.1016/j.jcou.2015.10.003

Ercolino G., Karimi S., Stelmachowski P., Specchia S. (2017). Catalytic combustion of residual methane on alumina monoliths and open cell foams coated with Pd/Co_3O_4. *Chem. Eng. J.*, Vol. 326, pp. 339-349. https://doi.org/10.1016/j.cej.2017.05.149

Ercolino G., Stelmachowski P., Specchia S. (2017). Catalytic performance of Pd/Co_3O_4 onSiC and ZrO_2 open cell foams for process intensification of methane combustion in lean conditions. *Ind. Eng. Chem. Res.*, Vol. 56, pp. 6625-6636. https://doi.org/10.1021/acs.iecr.7b01087

Fukuhara C., Hayakawa K., Suzuki Y., Kawasaki W., Watanabe R. (2017). A novel nickel based structured catalyst for CO_2 methanation: A honeycomb-type Ni/CeO_2 catalyst to transform greenhouse gas into useful resources. *Appl. Catal. A*, Vol. 532, pp. 12-18. https://doi.org/10.1016/j.apcata.2016.11.036

Groppi G., Beretta A., Tronconi E. (2005). Monolithic catalysts for gas-phase syntheses of chemicals" in *Structured catalysts and reactors.* 2nd ed., A. Cybulski and J.A. Moulijn, CRC Press. *Taylor & Francis Group*, pp. 243-310. https://doi.org/10.1016/j.cej.2017.05.149

Kim J. H., Suh D. J., Park T. J., Kim K. L. (2000). Effect of metal particle size on coking during CO_2 reforming of CH_4 over Ni–alumina aerogel catalysts. *Appl. Catal. A*, Vol. 197, No. 2, pp. 191-200. https://doi.org/10.1016/S0926-860X(99)00487-1

Li Y., Zhang Q., Chai R., Zhao G., Liu Y., Lu Y. (2015). Ni-Al_2O_3/Ni-foam catalyst with enhanced heat transfer for hydrogenation of CO_2 to methane. *AIChE J.*, Vol. 61, pp. 4323-4331. https://doi.org/10.1002/aic.14935

Parmar R. D., Kundu A., Karan K. (2009). Thermodynamic analysis of diesel reforming process: Mapping of carbon formation boundary and representative independent reactions. *J. Power Sources*, Vol. 194, No. 2, pp. 1007-1020. https://doi.org/10.1016/j.jpowsour.2009.06.028

Rostrup-Nielsen J. R., Pedersen K., Sehested J. (2007). High temperature methanation. Sintering and structure sensitivity. *Appl. Catal. A*, Vol. 330, pp. 134-138. https://doi.org/10.1016/j.apcata.2007.07.015

Sadykov V., Mezentseva N., Fedorova Y., Lukashevich A., Pelipenko V., Kuzmin V., Simonov M., Ishchenko A., Vostrikov Z., Bobrova L., Sadovskaya E., Muzykantov V., Zadesenets A., Smorygo O., Roger A. C., Parkhomenko K. (2015). Structured catalysts for steam/autothermal reforming of biofuels on heat-conducting substrates: Design and performance. *Catal. Today*, Vol. 251, pp. 19-27. https://doi.org/10.1016/j.cattod.2014.10.045

Song C., Pan W. (2004). Tri-reforming of methane: A novel concept for catalytic production of industrially useful synthesis gas with desired H_2/CO ratios. *Catal. Today*, Vol. 98, No. 4, pp. 463-484. https://doi.org/10.1016/j.cattod.2004.09.054

Specchia S., Ercolino G., Karimi S., Italiano C., Vita A. (2017). Solution combustion synthesis for preparation of structured catalysts: A mini-review on process intensification for energy applications and pollution control. *J. Self-Propag. High-Temp. Synth.*, Vol. 26, No. 3, pp. 166-186. https://doi.org/10.3103/S1061386217030062

Vita A., Cristiano G., Italiano C., Pino L., Specchia S. (2015). Syngas production by methane oxy-steam reforming on Me/CeO_2 (Me = Rh, Pt, Ni) catalyst lined on cordierite monoliths. *Appl. Catal. B*, Vol. 162, pp. 551-563. https://doi.org/10.1016/j.apcatb.2014.07.028

Vita A., Italiano C., Fabiano C., Pino L., Laganà M., Recupero V. (2016). Hydrogen-rich gas production by steam reforming of n-dodecane: Part I: Catalytic activity of Pt/CeO_2 catalysts in optimized bed configuration. *Appl. Catal. B*, Vol. 199, pp. 350-360. https://doi.org/10.1016/j.apcatb.2016.06.042

Vita A., Italiano C., Pino L., Frontera Ferraro P., M., Antonucci V. (2018). Activity and stability of powder and monolith-coated Ni/GDC catalysts for CO_2 methanation. *Appl. Catal. B*, Vol. 226, pp. 384-395. https://doi.org/10.1016/j.apcatb.2017.12.078

Wijaya W. Y., Kawasaki S., Watanabe H., Okazaki K. (2012). Damköhler number as a descriptive parameter in methanol steam reforming and its integration with absorption heat pump system. *Appl. Energy*, Vol. 94, pp. 141-147. https://doi.org/10.1016/j.apenergy.2012.01.041

Williams J. L. (2001). Monolith structures, materials, properties and uses. *Catal. Today*, Vol. 69, No. 1-4, pp. 3-9. https://doi.org/10.1016/S0920-5861(01)00348-0

Xu L., Yang H., Chen M., Wang F., Nie D., Qi L., Lian X., Chen H., Wu M. (2017). CO_2 methanation over Ca doped ordered mesoporous Ni-Al composite oxide catalysts: The promoting effect of basic modifier. *J. CO_2 Util.*, Vol. 21, pp. 200-210. https://doi.org/10.1016/j.jcou.2017.07.014

Zeppieri M., Villa P. L., Verdone N., Scarsella M., De Filippis P. (2010). Kinetic of methane steam reforming reaction over nickel-and rhodium-based catalysts. *Appl. Catal. A*, Vol. 387, No. 1-2, pp. 147-154. https://doi.org/ 10.1016/j.apcata.2010.08.017